


Article

# Coating of Titanium Substrates with $ZrO_2$ and $ZrO_2$ - $SiO_2$ Composites by Sol-Gel Synthesis for Biomedical Applications: Structural Characterization, Mechanical and Corrosive Behavior

Michelina Catauro <sup>1,\*</sup> , Federico Barrino <sup>1</sup>, Massimiliano Bononi <sup>2</sup>, Elena Colombini <sup>2</sup>, Roberto Giovanardi <sup>2</sup>, Paolo Veronesi <sup>2</sup> and Elisabetta Tranquillo <sup>1,\*</sup>

<sup>1</sup> Department of Engineering, University of Campania “Luigi Vanvitelli”, Via Roma 29, I-81031 Aversa, Italy; federicobarrino92@hotmail.it

<sup>2</sup> Department of Engineering “Enzo Ferrari”, University of Modena and Reggio Emilia, Via Vivarelli 10, 41125 Modena, Italy; massimiliano.bononi@unimore.it (M.B.); elena.colombini@unimore.it (E.C.); roberto.giovanardi@unimore.it (R.G.); paolo.veronesi@unimore.it (P.V.)

\* Correspondence: michelina.catauro@unicampania.it (M.C.); elisabetta.tranquillo@unicampania.it (E.T.)

Received: 26 February 2019; Accepted: 15 March 2019; Published: 19 March 2019



**Abstract:** The use of metallic materials as implants presents some major drawbacks, such as their harmful effects on the living organism, especially those induced by corrosion. To overcome this problem, the implant surface of titanium implants can be improved using a coating of bioactive and biocompatible materials. The aim of this work is the synthesis of  $SiO_2/ZrO_2$  composites with different percentages of zirconia matrix (20, 33 and 50 wt.%), by the sol-gel method to coat commercial Grade 4 titanium disks using a dip coater. Attenuated total reflectance Fourier transform infrared (ATR/FTIR) spectroscopy was used to evaluate the interactions between the inorganic matrices. Furthermore, the mechanical properties and corrosive behavior of the  $SiO_2/ZrO_2$  coatings were evaluated as a function of the  $ZrO_2$  content. The bioactive properties of the substrate coated with different composites were evaluated using simulated body fluid (SBF). The antibacterial activity was tested against gram-negative and gram-positive *Escherichia coli* and *Enterococcus faecalis*, respectively, to assess the release of toxic products from the different composites and to evaluate the possibility of using them in the biomedical field.

**Keywords:** sol-gel method; dip coating technique; composite materials; mechanical properties; corrosion behavior; bioactivity; antibacterial properties

## 1. Introduction

For many years now, the use of metallic materials for medical implants in traumatic, orthopedic and oral surgery has been known [1]. However, these materials, when used as implants, could present some damaging effects on the living organism, in particular, effects induced by corrosion. One of the most important factors for metallic medical implants is corrosion resistance, which limits the biocompatibility of implants due to the release of undesirable products in the body fluid, potentially also damaging mechanical properties in the organism [2,3].

To overcome this problem, the surface of titanium implants can be improved using a coating of bioactive and biocompatible materials [4–6]. Among the ceramic materials, zirconia was the first used in orthopedics as a substitute for titanium and alumina in hip head prostheses for its good mechanical and biological properties [7,8]. However, the transformation of the zirconia into different crystalline structures, as in the tetragonal to monoclinic phase, can be one of the main problems of its biological

application in living organisms, since this transformation induces roughening and breaking of the surface, which causes the implant to fail [9].

In the literature are some works related to the stabilization of the tetragonal phase of zirconia with silica, which may be better than other additives, because the silica does not affect the structure of zirconia [10–13]. Additionally, it is known that silica has a high corrosion resistance as well as good biological properties [14–17]. E. Długoń et al. [11] reported that ceramic coatings composed of zirconia and zirconia-silica were used to improve the corrosion resistance of titanium implants, while in the work of M.F. Morks et al. [18], zirconia and silica powders were mixed and plasma sprayed by using a gas tunnel plasma system to coat an SUS 304 substrate, and the microstructure, mechanical properties and in vitro behavior of the composite coatings were evaluated.

In this regard, the aim of this work has been to synthesize  $\text{SiO}_2/\text{ZrO}_2$  composites using the sol-gel method to coat commercial Grade 4 titanium disks using a dip coater. The sol-gel technique is a colloidal chemistry technology, which offers the possibility to synthesize various materials with chemical purity and predefined properties. Metal alkoxides are used in the synthesis procedure as precursors of the inorganic matrix. They are involved in hydrolysis and condensation reactions, producing bulk gels [19].

The sol-gel method can be coupled with coating techniques, such as dip, spin or spray coating. Many works show the importance of the sol-gel dip-coating technique, which is an ideal technology to coat many substrates with bioactive and biocompatible glassy materials to reduce corrosion, ion release and improve the bioactivity and biocompatibility of the substrate [20,21].

Ti-gr4 and nickel-titanium alloys are used in a wide range of biomedical applications, such as bone implants, stents and orthodontic wires [22,23]. Ti-gr4 has excellent mechanical properties and is resistant to corrosion, however, it is a bio-inert material. When introduced into biological tissues, the formation of peri-implant fibrosis can occur and isolate the implant from the surrounding bone and, therefore, lead to a reduction of implant performance [24]. Ni ions are produced by corrosion on the exposed surface of nickel-titanium alloys. The release of Ni ions is harmful to adjacent tissues around the implant [22]. To overcome these adverse characteristics, different alloys can be coated with sol-gel materials. In fact, in the biomedical field, mainly as orthopedic and dental implants, the use of sol-gel materials as coatings of metal implants to improve surface biological properties has been explored previously [23].

In this study, the new composites ( $\text{SiO}_2/\text{ZrO}_2$ ) with different percentages of zirconia matrix (20, 33 and 50 wt.%) were synthesized via the sol-gel method and were used to coat commercial Grade 4 titanium disks. The formation of interactions between the inorganic matrices was analyzed by attenuated total reflectance Fourier transform infrared (ATR/FTIR) spectroscopy.

Furthermore, the mechanical properties and corrosive behaviors of the  $\text{SiO}_2/\text{ZrO}_2$  coatings were evaluated as a function of the  $\text{ZrO}_2$  content. The bioactive properties of the substrate coated with different composites was evaluated using simulated body fluid (SBF).

Moreover, the antibacterial activity was tested against gram-negative and gram-positive *Escherichia coli* and *Enterococcus faecalis*, respectively, to assess the release of toxic products from the different composites and to evaluate the possibility of using them in the biomedical field.

## 2. Materials and Methods

### 2.1. Sol-Gel Synthesis and Coating

The new  $\text{SiO}_2/\text{ZrO}_2$  composites containing different percentages of zirconia (20, 33 and 50 wt.%) were synthesized by the sol-gel method. Tetraethyl orthosilicate (TEOS;  $\text{Si}(\text{OC}_2\text{H}_5)_4$ ; Sigma-Aldrich, Darmstadt, Germany) and a zirconium(IV) propoxide solution with 70 wt.% 1-propanol (Sigma-Aldrich, Darmstadt, Germany) were used as sources for the silica and zirconia matrix, respectively. First of all, the silica matrix was prepared by adding a solution of 99.8% ethanol (EtOH, Sigma-Aldrich, Darmstadt, Germany),  $\text{HNO}_3$  ( $\geq 65\%$ , Sigma-Aldrich, Darmstadt, Germany) and

distilled water, obtaining a sol with the following molar ratios between reagents:  $\text{H}_2\text{O}/\text{TEOS} = 2$ ,  $\text{EtOH}/\text{TEOS} = 6$ . Afterwards, different percentages of pure zirconia (20, 33 and 50 wt.%) were synthesized using a mixture of an alkoxide precursor, ethanol, water and acetylacetonate, which was used as an inhibitor agent against hydrolytic activity of the zirconium(IV) propoxide (AcAc, Sigma-Aldrich). Next, the zirconia sol was slowly added to the silica sol.

The zirconia sol presented the following molar ratios between reagents:  $(\text{Zr}(\text{OR})_4)/\text{AcAc} = 4.5$ ,  $\text{EtOH}/\text{Zr}(\text{OR})_4 = 5.7$ .

The synthesized  $\text{SiO}_2/\text{ZrO}_2$  composite materials were used to coat commercial Grade 4 titanium disks (Ti-4, Sweden and Martina, Padova, Italy) 8 mm in diameter and 2.20 mm thick, after 24 h of mixing the reagents. Before coating, the substrates were ultrasonically cleaned with acetone and subjected to a passivation process with  $\geq 65\%$   $\text{HNO}_3$  for 60 min. Subsequently, the KSV LM dip coater (KSV instruments Ltd., Helsinki, Finland) was used to coat the substrate with the synthesized composites. The withdrawal speed of the substrate used was kept to 15 mm/min. This process is illustrated in Figure 1. After the dip coating process, the sols were placed at room temperature and left to dry.

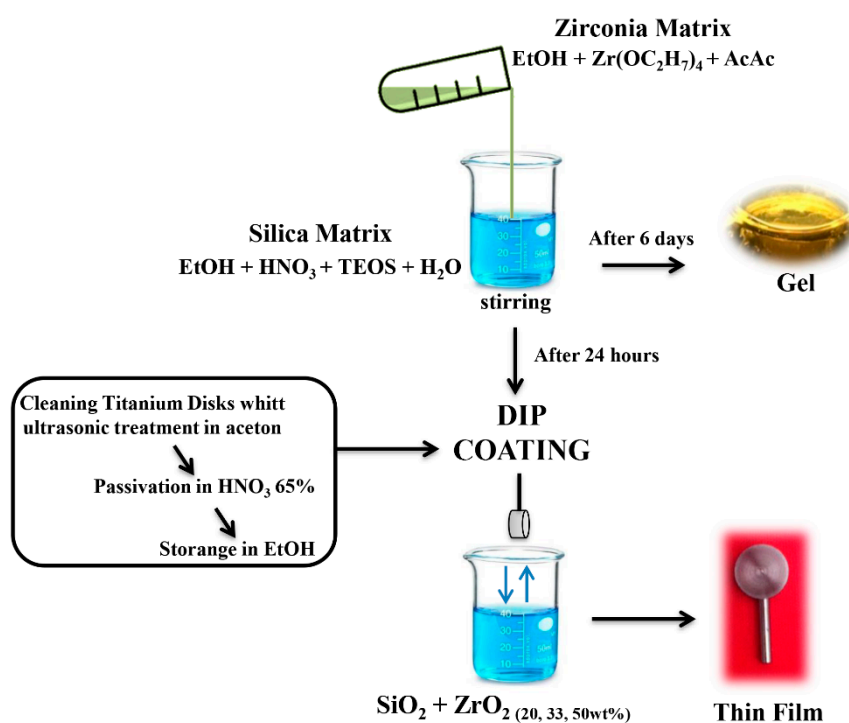


Figure 1. Flow chart of the process.

## 2.2. Coating Characterization

The chemical composition of the obtained coating surface was analyzed by attenuated total reflectance Fourier transform infrared (ATR/FTIR) spectroscopy (Tokyo, Japan). The spectra were obtained with the Prestige-21 FTIR spectrometer equipped with an AIM-8800 infrared microscope (Shimadzu Tokyo, Japan), using the incorporated 3-mm diameter Ge attenuated total reflectance (ATR) semicircular prism. Furthermore, the spectra were recorded with an incident angle of  $30^\circ$  with a resolution of  $4\text{ cm}^{-1}$  (64 scan) and were in the range of  $650\text{--}4000\text{ cm}^{-1}$ . The Prestige software (IRsolution, version 1.50) was used to further analyze the spectra.

## 2.3. Mechanical Characterization Techniques

Scratch tests have been carried out on a CSM Micro-Combi tester under progressive load conditions. In this test, a 1 mm scratch on the coating was made by drawing a diamond tip (Rockwell C

diamond scratch indenter with tip radius of 200  $\mu\text{m}$ ) on the surface and varying the normal load from 0.1 to 20 N at a loading rate of 19.92 N  $\text{min}^{-1}$ . The instrument is equipped with an integrated optical microscope, an acoustic emission detection system and a device measuring the tangential frictional force (along the scratch direction). The sensors provide information useful to determine the critical load for each coating-substrate assembly, in terms of the normal load at which the first incident of damage to the coating occurs. Three scratches were carried out in different zones for each specimen and the average value of the critical load was calculated.

Nanoindentation was performed using a Berkovitch indenter (Nanoindenter, CSM Instruments, Peseux, CH) operating at a constant load of 50 mN, applied for 15 s. This was done in order to maintain an indentation depth below 1  $\mu\text{m}$ . The nanoindentation results were analyzed according to the Oliver and Pharr procedure [25] in order to determine the coating hardness and elastic modulus. The penetration depth versus load curves have been used to calculate the amount of work required to perform the nanoindentation, and the percentage of work conducted in the elastic regime (integral of the unloading curve) or plastic regime (difference between the integral of the loading curve and the unloading curve). Ten nanoindentations were performed in different zones of each specimen, and the average values have been calculated.

#### 2.4. Corrosion Tests

The corrosion resistance was evaluated by potentiodynamic polarization tests and electrochemical impedance spectra analyses, performed in an electrochemical cell (Flat Cell K0235 PAR), using the samples as a working electrode (exposing an area of 1.4  $\text{cm}^2$ ), a platinum grid as a counter electrode and an Ag/AgCl/KCl(sat.) electrode (SSCE) as a reference electrode (all the potentials reported in this paper refer to this reference electrode). The electrolyte used for the corrosion tests was a Sigma Aldrich DPBS solution (Dulbecco's phosphate-buffered saline solution, pH 7.4) with the addition of 0.1  $\text{gL}^{-1}$  of  $\text{CaCl}_2$ , 0.1  $\text{gL}^{-1}$  of  $\text{MgCl}_2 \cdot 6\text{H}_2\text{O}$  and 0.05  $\text{gL}^{-1}$  of bovine serum albumin (BSA) at 37  $^\circ\text{C}$ . The polarization procedure was carried out as follows: Each sample was immersed in the test solution for 1 h before applying any polarization in order to stabilize its rest potential ( $E_r$ ). Then, potentiodynamic polarization scans were carried out with a scan rate of 5  $\text{mVs}^{-1}$  in the range from  $-0.8\text{V}$  (vs  $E_r$ ) to 3.0V (vs  $E_r$ ), using a PAR VersaStat 3 potentiostat.

Furthermore, impedance spectra were acquired for each sample just before the polarization scan (after the 1-hour immersion for the stabilization of  $E_r$ ) and just after with the following settings: A 100 kHz–1 Hz frequency range and an AC amplitude of 10 mV RMS (Root Mean Square), without DC polarization (i.e., 0 V vs  $E_r$ ). The spectra were fitted with the software ZSimpWin (version 3.50), adopting a R(CPE-R)(CPE-R) equivalent circuit (where CPE stands for constant phase element).

In addition to the four coated samples, i.e., 100%  $\text{ZrO}_2$  and  $\text{ZrO}_2 + 50, 66$  and 80 wt.% of  $\text{SiO}_2$ , an uncoated titanium sample was tested to assess the corrosive behavior of the bare titanium. The uncoated sample was subjected to the same passivation process used as pretreatment for the coated samples (with 65%  $\text{HNO}_3$  for 60 min). Every condition was tested with a single potentiodynamic test after having assessed the high reproducibility with the execution of duplicates on two samples.

The coating protection efficiency (%P.E.) provided together with the Tafel analysis in Table 3 has been calculated through the following relationship: %P.E. =  $[(I_{0\text{cor}} - I_{\text{cor}})/I_{0\text{cor}}] \times 100$ , where  $I_{0\text{cor}}$  is the corrosion current of the uncoated sample.

#### 2.5. Bioactivity Test

The Ti-4 uncoated disks, coated disks and the powder materials were soaked in simulated body fluid (SBF) to evaluate their bioactivity. The SBF was prepared from NaCl,  $\text{NaHCO}_3$ , KCl,  $\text{MgCl}_2$ , 1 M HCl,  $\text{CaCl}_2 \cdot 6\text{H}_2\text{O}$ , and  $\text{Na}_2\text{SO}_4$  (Sigma-Aldrich, St. Louis, MO, USA) with a concentration that was suggested by Kokubo [26] (Table 1). The pH of the buffer was adjusted to pH 7.4 using 1 M HCl. The different disks as well as the powders were soaked in the SBF solution, which was replaced every two



days to avoid the depletion of ionic species in the SBF caused by the nucleation of biominerals on the samples.

**Table 1.** Simulated body fluid (SBF) composition.

Formulation	Na <sup>+</sup>	K <sup>+</sup>	Mg <sup>2+</sup>	Ca <sup>2+</sup>	Cl <sup>-</sup>	HCO <sub>3</sub> <sup>-</sup>	HPO <sub>4</sub> <sup>2-</sup>	SO <sub>4</sub> <sup>2-</sup>	Buffer
Blood plasma	142.0	5.0	1.5	2.5	103.0	27.0	1.0	0.5	-
SBF	142.0	5.0	1.5	2.5	144.0	4.2	1.0	0.5	HEPES

After 21 days of exposure at 37 °C, the materials were removed and dried in a desiccator. The ability to form an apatite layer on the disks surface was studied by the Quanta 200 SEM (FEI, Eindhoven, Netherlands), equipped with an energy-dispersive X-ray (EDX) spectrometer. EDX analysis was performed in a “spot mode” in which the beam was localized on a single manually chosen area within the field of view.

The formation of the hydroxyapatite layer on the powders was evaluated by the Prestige 21 Shimadzu (Japan) FTIR instrument, which was equipped with a DTGS detector. The transmittance FTIR spectra were recorded over a wavenumber range of 4000–400 cm<sup>-1</sup> with resolution of 4 cm<sup>-1</sup> (45 scans). The FTIR spectra were processed by the Prestige software (IR solution).

### 2.6. Antibacterial Properties

The antibacterial properties of the Ti-4 disks coated with SiO<sub>2</sub>/ZrO<sub>2</sub> composites, containing different percentages of zirconia, were studied using gram-negative *Escherichia coli* (ATCC 25922) and gram-positive *Enterococcus faecalis* (ATCC 29212) [27]. A bacterial cell suspension of 10 × 10<sup>5</sup> CFU/mL was produced by diluting the bacterial culture in distilled water. *E. coli* and *E. faecalis* were inoculated in a Tryptone Bile X-Gluc (TBX) medium (Liofilchem, Italy) and in a Slanetz and Bartley Agar Base (Liofilchem, Italy), respectively.

Afterwards, the bacteria were incubated with the different Ti-4 coated disks for 24 h at 44 °C for *E. coli* and 48 h at 36 °C for *E. faecalis*. The microbial growth was evaluated by observing the diameter of the inhibition halo (ID). The obtained values are the mean standard (SD) deviation of measurements on the samples, which were analyzed three times.

## 3. Results

### 3.1. Coating Characterization: ATR-FTIR

In Figure 2, representative images of the Ti-4 disks (untreated and one coated with SiO<sub>2</sub>/ZrO<sub>2</sub> (33 wt.%)) can be seen. It is only possible to observe the different color of the disks. No other differences are visible due to the thin film thickness.



**Figure 2.** Representative images of the commercial Grade 4 titanium (Ti-4) disks: Untreated disk (left) and disk coated with SiO<sub>2</sub>/ZrO<sub>2</sub> (33 wt.%) (right).

The presence of the interactions between the two inorganic phases were investigated by means of ATR-FTIR spectroscopy. In Figure 3, the spectra of the different composites are reported. In the

spectrum of the silica matrix coating (curve e), the typical peaks of SiO<sub>2</sub> sol-gel materials are visible. The asymmetric and symmetric Si–O stretching vibrations can be attributed to the bands at 1060 cm<sup>−1</sup> and 790 cm<sup>−1</sup> [28]. Furthermore, the peaks at 1640 cm<sup>−1</sup> and 952 cm<sup>−1</sup> are due to –OH bending vibrations in the water and Si–OH bonds vibrations, respectively [29]. The zirconia matrix spectra (curve a) show that the bands at 1530 cm<sup>−1</sup> and 1285 cm<sup>−1</sup> are assigned to the C–C vibrations and that the peak at 1365 cm<sup>−1</sup> is due to C=O vibrations of AcAc bidentate binding. Methyl C–H symmetric bending is visible at 1415 cm<sup>−1</sup>. Moreover, the peak at 1020 cm<sup>−1</sup> can be attributed to C–C–H bending, mixed with stretching C–C vibrations of AcAc [30]. Also, in the spectrum of the zirconia matrix, –OH bending vibrations in the water at 1655 cm<sup>−1</sup> are present.

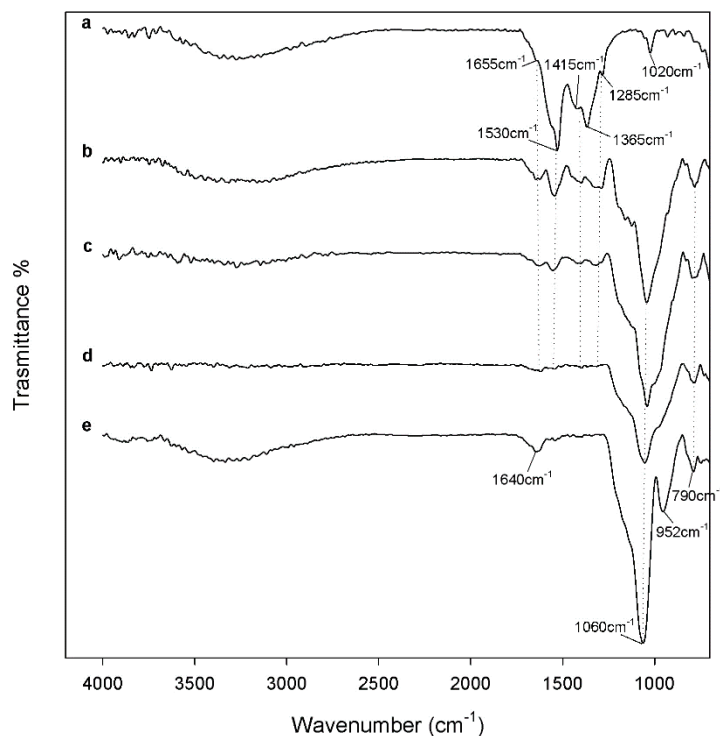
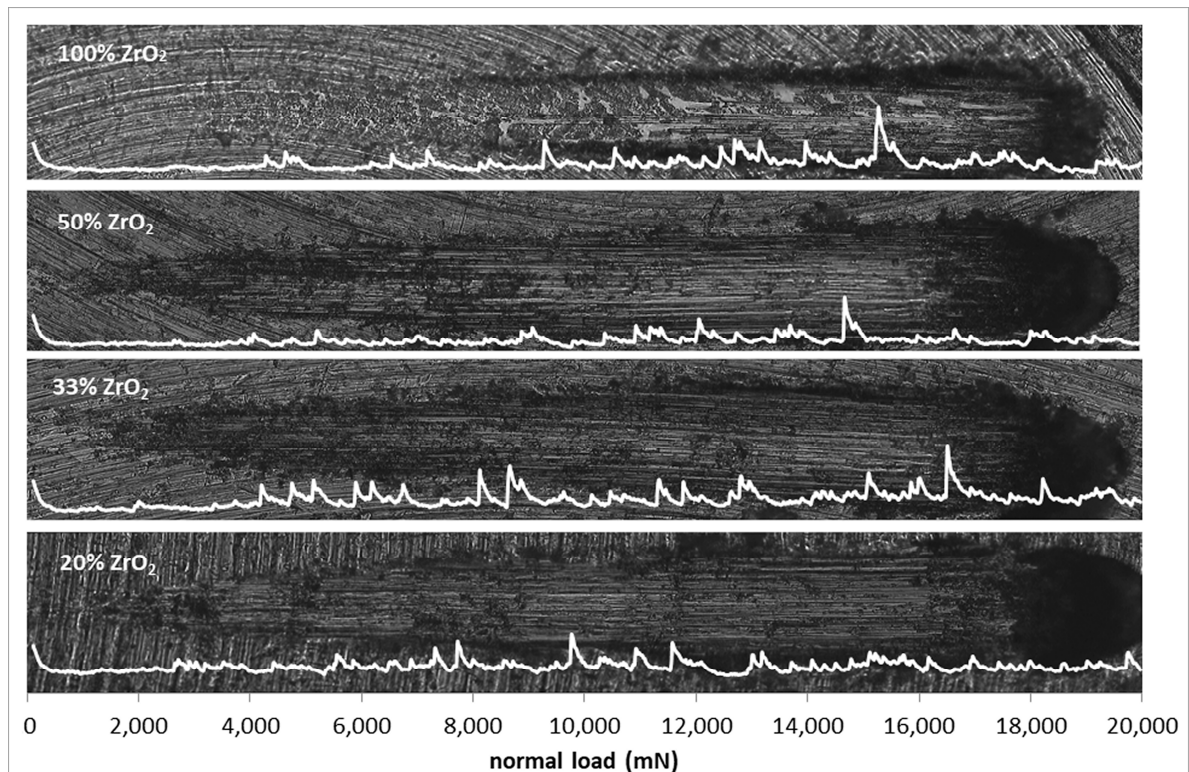


**Figure 3.** Attenuated total reflectance Fourier transform infrared (ATR-FTIR) spectroscopy spectra of (a) pure ZrO<sub>2</sub>, (b) 50 wt.% SiO<sub>2</sub>/ZrO<sub>2</sub>, (c) 33 wt.% SiO<sub>2</sub>/ZrO<sub>2</sub>, (d) 20 wt.% SiO<sub>2</sub>/ZrO<sub>2</sub> and (e) pure SiO<sub>2</sub>.

Comparing the spectra of the coating composites with different amounts of the zirconia matrix (20, 33 and 50 wt.%), it is possible to observe a change in the shape and intensity of some peaks, such as the band at 1650 cm<sup>−1</sup>. The displacement of the Si–O stretching band at a lower wavenumber and the different shape is due to the higher incorporation of zirconia matrix. In the composite spectra (curves b, c and d), the slight shift of the peak at 790 cm<sup>−1</sup> can be attributed to the presence of Si–O–Zr interactions in the materials [31]. Furthermore, the formation of the interactions between the silica and zirconia matrix are confirmed by the change in intensity of the silanol band at 952 cm<sup>−1</sup> [32]. In fact, if the number of bonds increases, the number of silanol the groups decreases. As a result, the intensity at 952 cm<sup>−1</sup> would decrease or completely disappear [33].

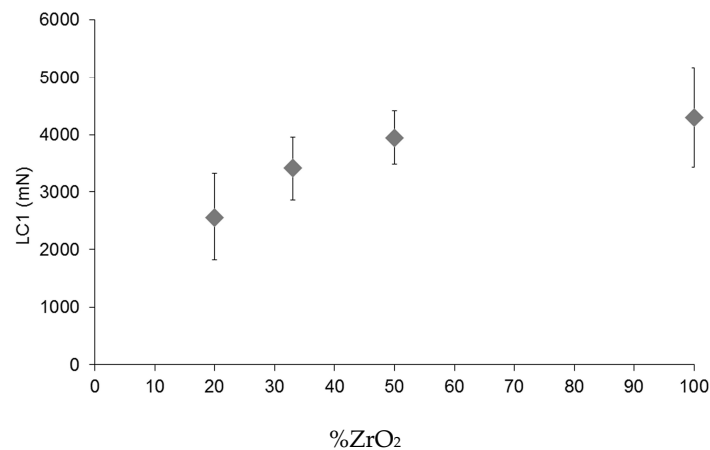
### 3.2. Mechanical Characterization Techniques

Figure 4 shows a set of optical microscope micrographs of scratch tests performed on samples containing 20, 33, 50 and 100% ZrO<sub>2</sub>, with superimposed the acoustic emission signal as a function of the applied normal load.



**Figure 4.** Scratch test micrographs and the overlaid recorded acoustic emission for samples containing 20, 33, 50 and 100% zirconia. Silica = bal.

The measured values of critical load, determined both optically and based on the acoustic emission signal, indicated as LC1, are summarized in Figure 5 below.



**Figure 5.** Results of scratch tests: Critical load (LC1).

The SiO<sub>2</sub>-free coatings present the highest value of critical load, despite a severe scattering of the results. The trend is non-linear and the addition of 50% ZrO<sub>2</sub> is particularly effective at increasing the critical load. However, the introduction of high percentages of zirconia affects the mechanisms of damaging the coatings. Figure 6 shows a comparison of the coating surface for a normal load centered around 9000 mN, where extensive damage occurs. The 100% ZrO<sub>2</sub> containing sample presents delamination and detachment of the coating from the underlying titanium substrate, while the 33% one is still adhered and presents a large number of cracks extending outward from the scratch region.

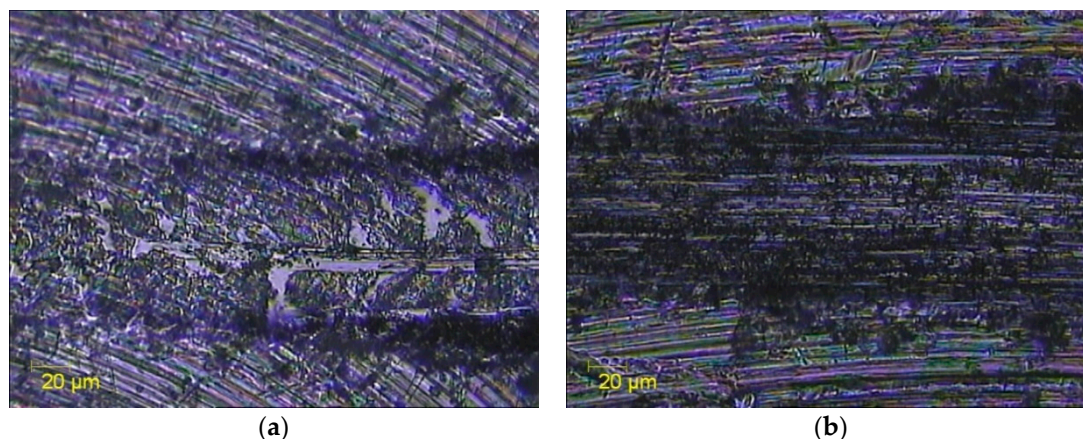


**Figure 6.** Scratch micrographs at a normal load of 9000 mN, showing extensive damage (from left to right): (a) 100% ZrO<sub>2</sub> coating; (b) 33% ZrO<sub>2</sub> coating.

Table 2 shows the measured hardness, expressed in equivalent HV (Hardness in Vickers scale) and the calculated Young modulus of the coating as a function of the ZrO<sub>2</sub> content. The table includes also the amount of energy required to run the nanoindentation and the percentage in the elastic or plastic field:

**Table 2.** Hardness of the coatings (HV), Young's modulus (E), plastic work and percentages in the elastic (%el) or plastic (%pl) field, determined by nanoindentation as a function of ZrO<sub>2</sub> content (average values, Avg, and Standard deviations, SD, are reported).

Coatings Mechanical Properties	20% ZrO <sub>2</sub>		33% ZrO <sub>2</sub>		50% ZrO <sub>2</sub>		100% ZrO <sub>2</sub>	
	Avg	SD	Avg	SD	Avg	SD	Avg	SD
HV	283.67	33.50	303.39	38.05	340.00	74.22	367.67	42.16
E (GPa)	61.81	25.79	64.95	9.41	72.60	5.76	117.00	9.17
Energy (pJ)	19,842	2789	17,002	822	16,509	620	16,076	1203
%el	25.68%	6.12%	27.84%	1.87%	27.51%	1.93%	18.45%	1.01%
%pl	74.32%	6.12%	72.16%	1.87%	72.49%	1.93%	81.55%	1.01%

The nanoindentation results confirm the expected trend of an increasing hardness and Young's modulus as the percentage of zirconia increases. However, the measured results are significantly lower than the ones of the bulk zirconia and silica-zirconia materials, however, they are in agreement with the literature results [34]. This could be ascribed to the indentation conditions, which did not allow the ability to stress the coating alone. Rather interestingly, the lower energy required to run the indentation on the 100% ZrO<sub>2</sub> sample and the lower percentage in the elastic field is in agreement with the observed behavior of a higher tendency of richer zirconia coatings to undergo extensive cracking (a lower energy is elastically recovered after the indentation due to the crack formation and propagation). The generally high values of the work in the plastic fields suggests that, in all cases, severe cracking (i.e., non-recoverable deformation) occurred, in agreement with the scratch test results.

It can be concluded that ZrO<sub>2</sub>-rich coatings generally present a higher critical load during scratch testing and are stiffer, but with a greater tendency to crack. The coatings containing higher percentages of SiO<sub>2</sub> instead are softer but can recover from a slightly higher amount of deformation work and in general present a better adhesion to the substrate.

### 3.3. Corrosion Tests

Figure 7 shows the potentiodynamic polarization plots, in a DPBS + BSA solution, of the passivated bare and coated Ti-4 disks with different relative percentages of ZrO<sub>2</sub> and SiO<sub>2</sub>. Tafel analysis was been performed on the potentiodynamic plots and the results are provided in Table 3, together with the calculated protection efficiency of every coating. The present discussion will focus



on the comparison of the passivation phenomena, since every material exhibited passive behavior. The uncoated Ti-4 (grey plot) showed a trend analogous to that reported in literature for Ti alloys in the same media [35,36]. In particular, it showed a corrosion potential of approximately  $-0.4$  V (SSCE), a first passivation range between  $-0.3$  V and  $0.5$  V (with a very low passive current density of  $0.1$ – $0.3 \mu\text{Acm}^{-2}$ ) and a second one beyond approximately the potential of  $1$  V, where a still low current density between  $20$  and  $50 \mu\text{Acm}^{-2}$  was preserved. Comparing the uncoated sample with the coated ones, it can be noticed that all the coatings show an analogous behavior (same trend of the plot), but all of them show a significant decrease of the corrosion current in the first passivation range. This current decrease of about one order of magnitude confirms the presence of a compact layer which hampers the flow of electrolytes through it, making it more insulated and therefore more corrosion resistant. After this first range, beyond  $0.4$ – $0.7$  V, all the trends become practically identical to those of the uncoated Ti-4. Therefore, beyond this potential threshold, the coating completely loses its extra corrosion-protective properties. The samples still maintain the same good protection of the passivated Ti-4, showing that the production process of the coating does not affect the passivation layer on the Ti-4 substrate. A comparison among the coated samples showed that higher protection (lower current density) was provided when the coating composition was purer. Indeed, the lowest current density was obtained with the  $100\%$   $\text{ZrO}_2$ , followed by the  $80\%$   $\text{SiO}_2$  and  $20\%$   $\text{ZrO}_2$ . When the composition increasingly moves away from pure  $\text{ZrO}_2$  or pure  $\text{SiO}_2$  (i.e., when the composition is mixed) the current slightly increases. Apparently, as far as corrosion protection is concerned, the interaction between  $\text{ZrO}_2$  and  $\text{SiO}_2$  obtained in these conditions is not optimal, although the worsening is slight anyhow. As a confirmation, the scratch tests previously discussed showed that pure  $\text{ZrO}_2$  tended to detach from the Ti-4 substrate when subjected to load, while the mixed coatings were characterized by diffused cracks. A coating detachment under mechanical stress is not favorable, but it may confirm the great compactness of the coating itself. Since corrosion tests do not involve mechanical stress and so do not hamper coating compactness, a higher protection in  $100\%$   $\text{ZrO}_2$  is found. On the other hand, mixed coatings are more subject to cracking (due to being less compact), although mechanically they perform better due to a higher coating adherence. Mixed coatings offer more possibility to be penetrated by the electrolyte through micro cracks which should be present on the samples, resulting in a slightly higher corrosive current density. The difference among the coatings, in terms of corrosion resistance, is small, and it can be concluded that all of the coatings provide an additional protective layer which increases the already high corrosion resistance of uncoated Ti-4 in this environment.

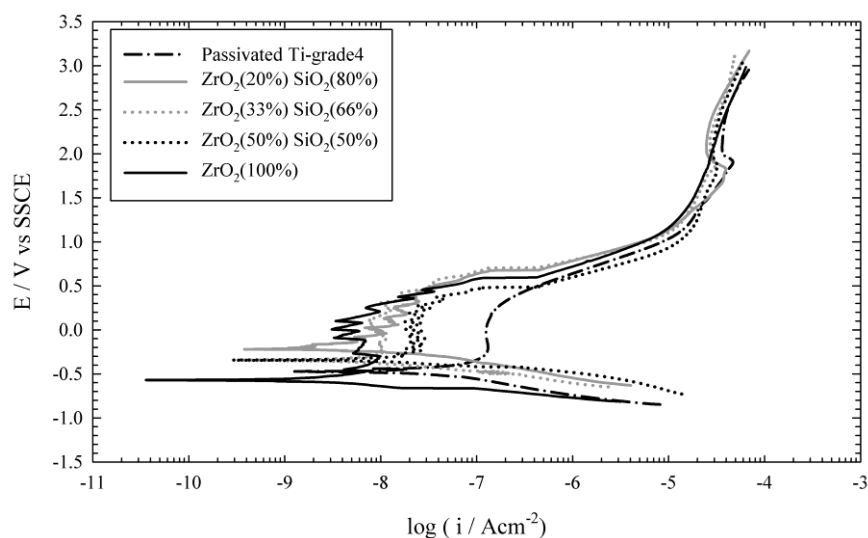


**Figure 7.** Potentiodynamic polarizations performed in a DPBS + BSA electrolyte on the bare passivated Ti-4 disk and on disks coated with 20 wt.%  $\text{SiO}_2/\text{ZrO}_2$ , 33 wt.%  $\text{SiO}_2/\text{ZrO}_2$ , 50 wt.%  $\text{SiO}_2/\text{ZrO}_2$  and pure  $\text{ZrO}_2$ .



**Table 3.** Corrosion currents ( $I_{cor}$ ) and corrosion potentials ( $E_{cor}$ ), calculated via Tafel analysis on the potentiodynamic plots of the different samples and their corresponding protection efficiency (%P.E.).

Tafel Analysis Results	$I_{cor}$ [ $Acm^{-2}$ ]	$E_{cor}$ [V versus SSCE]	%P.E.
Passivated Ti-4	$2.31 \times 10^{-8}$	-0.483	-
ZrO <sub>2</sub> (20%) SiO <sub>2</sub> (80%)	$1.99 \times 10^{-9}$	-0.178	91%
ZrO <sub>2</sub> (33%) SiO <sub>2</sub> (66%)	$5.57 \times 10^{-9}$	-0.344	76%
ZrO <sub>2</sub> (50%) SiO <sub>2</sub> (50%)	$8.92 \times 10^{-9}$	-0.344	61%
ZrO <sub>2</sub> (100%)	$1.80 \times 10^{-9}$	-0.582	92%

In Figure 8, the impedance spectra acquired before and after the polarization are shown in a Nyquist plot. In Table 4, the results of the spectra fitted adopting a R(CPE-R)(CPE-R) equivalent circuit are provided. In particular, only the uncoated Ti, the 100% ZrO<sub>2</sub> (the most performing coating in the polarization results) and the 50% SiO<sub>2</sub> and 50% ZrO<sub>2</sub> (the least performing among the coated ones) are shown, in order to make an overall comparison between the trends and confirm the previous results of the polarizations.

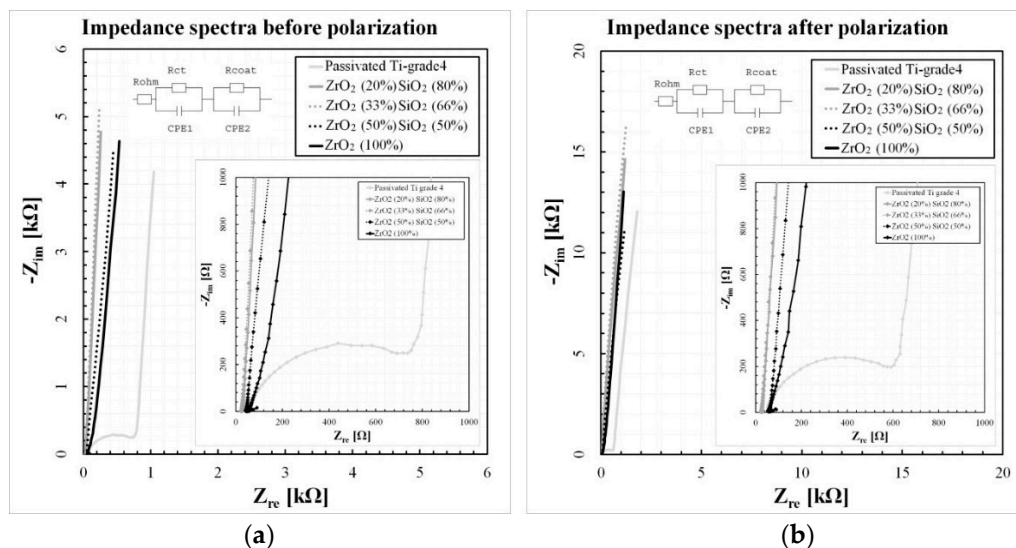


**Figure 8.** Electrochemical impedance spectra acquired in a DPBS + BSA electrolyte, before and after the potentiodynamic polarizations, on the bare passivated Ti-4 disk and on disks coated with 20 wt.% SiO<sub>2</sub>/ZrO<sub>2</sub>, 33 wt.% SiO<sub>2</sub>/ZrO<sub>2</sub>, 50 wt.% SiO<sub>2</sub>/ZrO<sub>2</sub> and pure ZrO<sub>2</sub>: Overall and zoom. (a) spectra acquired before the polarizations; (b) spectra acquired after the polarizations.

**Table 4.** Results of the fitting procedure performed on the impedance spectra adopting a R(CPE-R)(CPE-R) equivalent circuit.

EIS Spectra Fitting Results	$R_{ohm}$ [ $\Omega$ ]	$R_{ct}$ [ $\Omega$ ]	$Y_{0d1}$ [ $F s^{n-1}$ ]	$n_{d1}$ [—]	$R_{coating}$ [ $\Omega$ ]	$Y_{0coating}$ [ $F s^{n-1}$ ]	$n_{coating}$ [—]	$\chi^2$
Passivated Ti-4 (before)	45.5	784.8	$4.95 \times 10^{-6}$	0.75	$1.6 \times 10^5$	$3.86 \times 10^{-5}$	0.98	$1.7 \times 10^{-4}$
Passivated Ti-4 (after)	44.8	602.1	$1.54 \times 10^{-6}$	0.80	$3.7 \times 10^5$	$1.39 \times 10^{-5}$	0.95	$2.7 \times 10^{-4}$
ZrO <sub>2</sub> 100% (before)	51.9	309.1	$4.64 \times 10^{-4}$	0.60	$1.7 \times 10^5$	$3.53 \times 10^{-5}$	0.98	$9.6 \times 10^{-5}$
ZrO <sub>2</sub> 100% (after)	50.3	224.0	$3.45 \times 10^{-4}$	0.56	$1.8 \times 10^6$	$1.29 \times 10^{-5}$	0.96	$1.4 \times 10^{-4}$
SiO <sub>2</sub> 50% ZrO <sub>2</sub> 50% (before)	41.7	4.9	$3.41 \times 10^{-4}$	0.70	$5.7 \times 10^5$	$3.83 \times 10^{-5}$	0.94	$5.2 \times 10^{-5}$
SiO <sub>2</sub> 50% ZrO <sub>2</sub> 50% (after)	56.4	9.3	$1.96 \times 10^{-4}$	0.68	$4.4 \times 10^5$	$1.50 \times 10^{-5}$	0.95	$1.0 \times 10^{-4}$

As visible in the graphs, every plot is characterized by a high slope, confirming the presence of a high-resistance coating. Indeed, the  $R_{coating}$  values shown in Table 4 are in the order of 100–1000 k $\Omega$ . In the uncoated Ti, the element  $R_{coating}$  simulates the effect of the passivation oxide layer, while in the coated samples, it simulates the combined effect of both the passivation layer and the SiO<sub>2</sub>/ZrO<sub>2</sub> coating. Looking at the  $R_{coating}$  values after the polarization, the same behavior encountered in the potentiodynamic tests is found: The 100% ZrO<sub>2</sub> shows the highest resistance (highest coating

compactness), followed by the 50% SiO<sub>2</sub> and 50% ZrO<sub>2</sub>, which however improves when compared to the uncoated Ti.

### 3.4. Bioactivity Test

The powders of the SiO<sub>2</sub>/ZrO<sub>2</sub> composites, with different percentages of zirconia matrices, were soaked in a SBF solution for 21 days. When the several composites were soaked in SBF solution, the presence of Si–OH and Zr–OH on the materials surfaces allows the interaction of both matrix functional groups with the ions present in the SBF solution, in particular with Ca<sup>2+</sup>, and afterwards with phosphate ions. The Ca<sup>2+</sup> ions combine with the negative charge of the phosphate ions, inducing the formation of hydroxyapatite layer [Ca<sub>10</sub>(PO<sub>4</sub>)<sub>6</sub>(OH)<sub>2</sub>] [37,38].

In order to evaluate the formation of hydroxyapatite layer, FTIR spectroscopy was used. In Figure 3, the spectra of the composites after 21 days of exposure to SBF are reported. Comparing the pure SiO<sub>2</sub> and SiO<sub>2</sub>/ZrO<sub>2</sub> (50wt.%) spectra (Figure 3, curves a and g) recorded before being soaked in the solution with the spectra of all materials after 21 days in SBF, new peaks appear in the spectra range of 600–500 cm<sup>−1</sup>.

In Figure 9, the split of the band at 565 cm<sup>−1</sup> (curve a) into two new ones at 587 cm<sup>−1</sup> and 553 cm<sup>−1</sup> (curve b) was observed. Furthermore, these two new peaks are visible in the material composite spectra, and also the displacement of others peaks in the spectra range of 600 cm<sup>−1</sup>, which are due to the stretching of –OH groups of hydroxyapatite and the vibrations of the PO<sub>4</sub><sup>3−</sup> groups, caused by the interaction among the hydroxyapatite precipitate and the matrix [39].

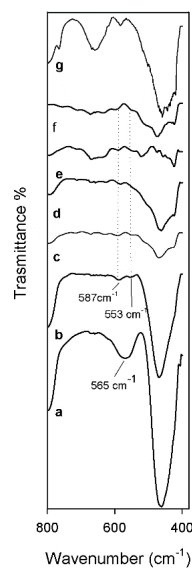


**Figure 9.** FT-IR spectra of (a) pure SiO<sub>2</sub> not soaked in SBF; (b) pure SiO<sub>2</sub>; (c) SiO<sub>2</sub>/ZrO<sub>2</sub> (20 wt.%); (d) SiO<sub>2</sub>/ZrO<sub>2</sub> (33 wt.%); (e) SiO<sub>2</sub>/ZrO<sub>2</sub> (50 wt.%); (f) pure ZrO<sub>2</sub> after 21 days in SBF; (g) SiO<sub>2</sub>/ZrO<sub>2</sub> (50 wt.%), not soaked in SBF.

Therefore, the bioactivity of Ti-4 disks coated with SiO<sub>2</sub>/ZrO<sub>2</sub> composites was investigated by SEM. Comparing the SEM micrographs of the materials after 21 days of exposure to SBF (Figure 9b–d) no difference in the apatite layer was observed, in fact, the surfaces of the materials were covered by a precipitate with the globular shape, typical of hydroxyapatite. The energy-dispersive X-ray (EDX) microanalysis of the different composites, after 21 days in SBF, confirmed that the atomic ratio between Ca and P was equal to 1.67, furthermore, the other peaks were residuals from the sample preparation and SBF solution (Figure 10e). The signs of Zr or Si are not visible in the EDX analysis due to the strong peak intensity of the P that covers them.

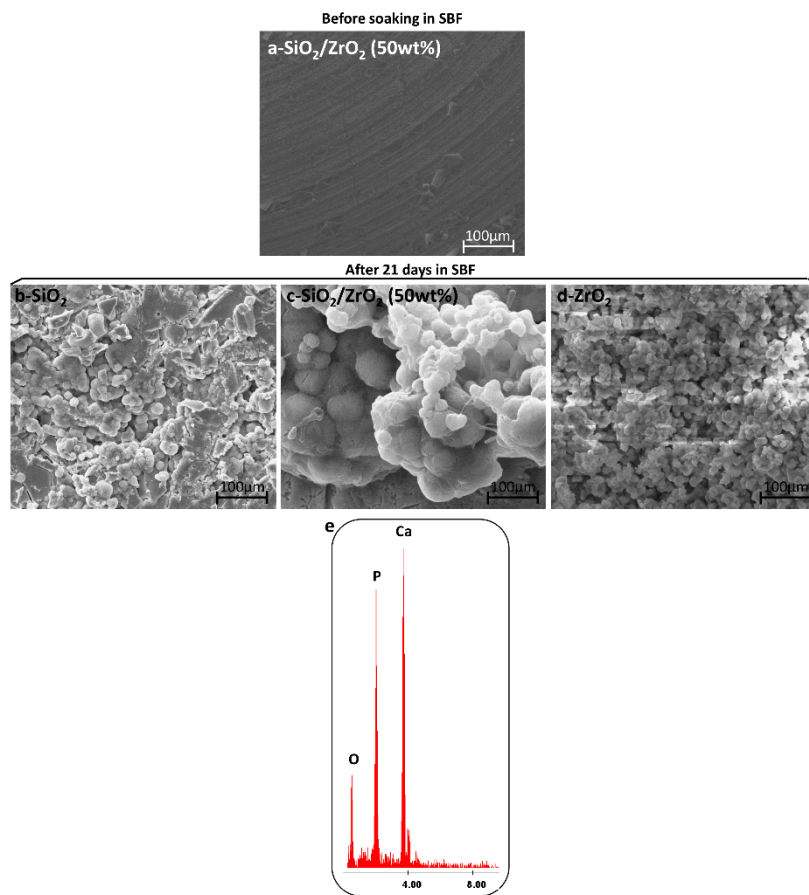


**Figure 10.** SEM micrographs of (a) the representative  $\text{SiO}_2/\text{ZrO}_2$  (50 wt.%) composite; (b) pure  $\text{SiO}_2$ ; (c)  $\text{SiO}_2/\text{ZrO}_2$  (50 wt.%) composite; (d) pure  $\text{ZrO}_2$  after 21 days in SBF. (e) EDX analysis of the  $\text{SiO}_2/\text{ZrO}_2$  (50 wt.%) composite.

### 3.5. Antibacterial Properties

The Ti-4 disks coated with  $\text{SiO}_2/\text{ZrO}_2$  composites, containing 20, 33 and 50 wt.%  $\text{ZrO}_2$ , were incubated with gram-positive and gram-negative bacterial strains. Figure 11A reports a representative image of *E. faecalis*, while the progress of bacterial growth is shown in Figure 11B. When the thin films were inoculated for 24 h with *E. coli* and 48 h with *E. faecalis*, the inhibition halo (ID) was not observed, regardless of the  $\text{ZrO}_2$  content.

It is likely that no toxic products were released from the different coatings, allowing the growth of bacteria. The results suggest that the zirconia pure coating, as well as the Ti-4 disks coated with  $\text{SiO}_2/\text{ZrO}_2$ , independent of the zirconia percentages, do not have toxic effects against gram-positive and gram-negative bacterial strains.

Therefore,  $\text{SiO}_2/\text{ZrO}_2$  composites may be used as non-toxic coating materials.

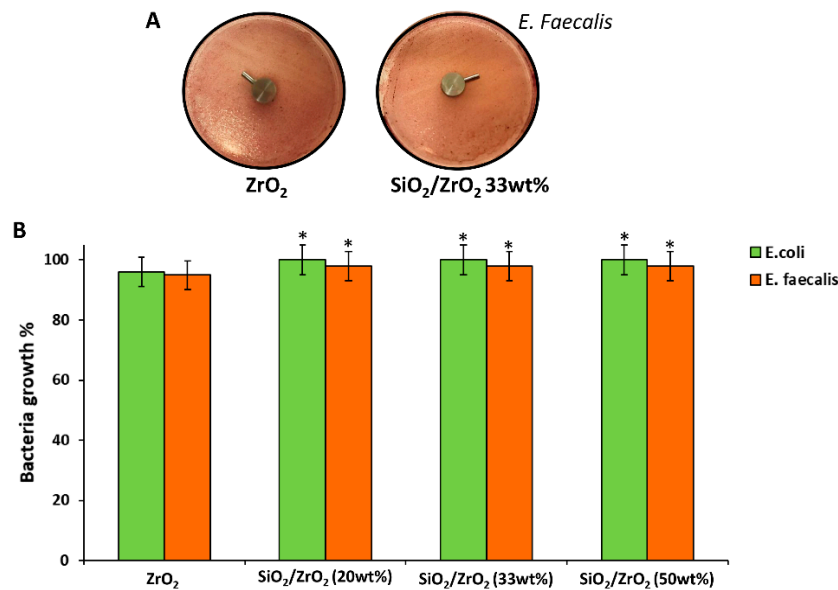


**Figure 11.** (A) Representative image of *E. faecalis* incubated with Ti-4 disks coated with ZrO<sub>2</sub> and SiO<sub>2</sub>/ZrO<sub>2</sub> (33 wt.%). (B) Bacteria growth (%) of *E. coli* and *E. faecalis* incubated with ZrO<sub>2</sub>, SiO<sub>2</sub>/ZrO<sub>2</sub> (20 wt.%), SiO<sub>2</sub>/ZrO<sub>2</sub> (33 wt.%) and SiO<sub>2</sub>/ZrO<sub>2</sub> (50 wt.%). Values are the mean standard deviation of measurements carried out on samples analyzed three times. The means and standard deviations are shown. \*,  $p < 0.05$  versus the bacteria treated with different composites.

#### 4. Conclusions

In this work, different ZrO<sub>2</sub>/SiO<sub>2</sub>-based coatings obtained on a Ti-4 substrate via sol-gel synthesis for biomedical applications have been studied, with regard to their structure, corrosion resistance and mechanical and bioactive behaviors. The following conclusions can be made:

- ATR-FTIR spectroscopy suggests that interaction between both inorganic matrixes occurred.
- FTIR spectra and SEM/EDX analysis showed the same bioactivity among all materials, in fact, the bioactive proprieties are due to a synergy between both inorganic components.
- A decrease of the bacterial growth was not observed when the Ti-4 disks coated with SiO<sub>2</sub>/ZrO<sub>2</sub> composites were incubated with gram-negative and gram-positive bacteria, suggesting that the coating materials are non-toxic and could be used in clinical applications.
- All the coatings improved the corrosion resistance of the Ti substrate, as all the coated samples showed an evident decrease of corrosion current density in the passivation region of the potentiodynamic curves.
- As far as the mechanical properties are concerned, the SiO<sub>2</sub>-containing coatings showed the best performances due to a better adhesion to the Ti substrate, as proved by the scratch tests.
- On the other hand, the SiO<sub>2</sub>-containing coatings did not show the absolute best results in the corrosion tests because of the presence of microcracks which allow the electrolyte to come into contact with the substrate underneath.
- Considering the SiO<sub>2</sub>-containing coatings performed best in the scratch tests, they can be considered as the best compromise between corrosion resistance and mechanical properties.

However, the difference between the coatings in terms of corrosion resistance and bioactivity is small. Probably all of the materials can be considered as useful in the biomedical field.

**Author Contributions:** Validation, M.C.; Formal analysis, F.B, M.B. and E.C.; Data curation, R.G. and P.V.; Writing—original draft preparation, M.C. and E.T.; Supervision, M.C.

**Funding:** This research received no external funding.

**Conflicts of Interest:** The authors declare no conflict of interest.

## References

1. Neoh, K.; Shi, Z.; Kang, E. Anti-adhesive and antibacterial polymer brushes. In *Biomaterials Associated Infection*; Springer: Berlin, Germany, 2013; pp. 405–432.
2. Balamurugan, A.; Rajeswari, S.; Balossier, G.; Rebelo, A.; Ferreira, J. Corrosion aspects of metallic implants—An overview. *Mater. Corros.* **2008**, *59*, 855–869. [[CrossRef](#)]
3. Manivasagam, G.; Dhinasekaran, D.; Rajamanickam, A. Biomedical implants: Corrosion and its prevention—a review. *J. Recent Patents Corros. Sci.* **2010**. [[CrossRef](#)]
4. Asri, R.; Harun, W.; Samykano, M.; Lah, N.; Ghani, S.; Tarlochan, F.; Raza, M. Corrosion and surface modification on biocompatible metals: A review. *J. Mater. Sci. Eng. C* **2017**, *77*, 1261–1274. [[CrossRef](#)]
5. Catauro, M.; Bollino, F.; Papale, F. Biocompatibility improvement of titanium implants by coating with hybrid materials synthesized by sol-gel technique. *J. Biomed. Mater. Res. Part A* **2014**, *102*, 4473–4479. [[CrossRef](#)] [[PubMed](#)]
6. Catauro, M.; Bollino, F.; Papale, F.; Gallicchio, M.; Pacifico, S. Synthesis and chemical characterization of new silica polyethylene glycol hybrid nanocomposite materials for controlled drug delivery. *J. Drug Deliv. Sci. Technol.* **2014**, *24*, 320–325. [[CrossRef](#)]
7. Coli, P.; Karlsson, S. Fit of a new pressure-sintered zirconium dioxide coping. *Int. J. Prosthodont.* **2004**, *17*, 59–64. [[PubMed](#)]
8. Evans, A.; Heuer, A. Transformation toughening in ceramics: Martensitic transformations in crack-tip stress fields. *J. Am. Ceram. Soc.* **1980**, *63*, 241–248. [[CrossRef](#)]
9. Soon, G.; Pinguan-Murphy, B.; Lai, K.W.; Akbar, S.A. Review of zirconia-based bioceramic: Surface modification and cellular response. *J. Ceram. Int.* **2016**, *42*, 12543–12555. [[CrossRef](#)]
10. Pessoa, R.; Cerqueira, M.; Nasar, R.; Yoshida, I. Synthesis of stabilized zirconia without dopants. *Cerâmica* **2008**, *54*, 253–258. [[CrossRef](#)]
11. Długoń, E.; Pach, K.; Gawęda, M.; Jadach, R.; Wajda, A.; Leśniak, M.; Benko, A.; Dziadek, M.; Sowa, M.; Simka, W. Anticorrosive ZrO<sub>2</sub> and ZrO<sub>2</sub>-SiO<sub>2</sub> layers on titanium substrates for biomedical applications. *Surf. Coat. Technol.* **2017**, *331*, 221–229. [[CrossRef](#)]
12. Ciesielczyk, F.; Goscińska, J.; Zdzarta, J.; Jesionowski, T. The development of zirconia/silica hybrids for the adsorption and controlled release of active pharmaceutical ingredients. *Colloids Surf. A* **2018**, *545*, 39–50. [[CrossRef](#)]
13. Fu, L.; Wu, C.; Grandfield, K.; Unosson, E.; Chang, J.; Engqvist, H.; Xia, W. Transparent single crystalline ZrO<sub>2</sub>-SiO<sub>2</sub> glass nanoceramic sintered by SPS. *J. Eur. Ceram. Soc.* **2016**, *36*, 3487–3494. [[CrossRef](#)]
14. Catauro, M.; Dell'Era, A.; Vecchio Cipriotti, S. Synthesis, structural, spectroscopic and thermoanalytical study of sol-gel derived SiO<sub>2</sub>-CaO-P<sub>2</sub>O<sub>5</sub> gel and ceramic materials. *Thermochim. Acta* **2016**, *625*, 20–27. [[CrossRef](#)]
15. Nguyen, K.; Garcia, A.; Sani, M.A.; Diaz, D.; Dubey, V.; Clayton, D.; Dal Poggetto, G.; Cornelius, F.; Payne, R.J.; Separovic, F.; et al. Interaction of N-terminal peptide analogues of the Na<sup>+</sup>,K<sup>+</sup>-ATPase with membranes. *Biochim. Biophys. Acta Biomembr.* **2018**, *1860*, 1282–1291. [[CrossRef](#)] [[PubMed](#)]
16. Catauro, M.; Tranquillo, E.; Salzillo, A.; Capasso, L.; Illiano, M.; Sapio, L.; Naviglio, S. Silica/Polyethylene glycol hybrid materials prepared by a sol-Gel method and containing chlorogenic acid. *Molecules* **2018**, *23*. [[CrossRef](#)]
17. Tranquillo, E.; Barrino, F.; Dal Poggetto, G.; Blanco, I. Sol-gel synthesis of silica-based materials with different percentages of PEG or PCL and high chlorogenic acid content. *Materials* **2019**, *12*. [[CrossRef](#)]
18. Morks, M.; Kobayashi, A. Development of ZrO<sub>2</sub>/SiO<sub>2</sub> bioinert ceramic coatings for biomedical application. *J. Mech. Behav. Biomed. Mater.* **2008**, *1*, 165–171. [[CrossRef](#)]
19. Brinker, C.; Scherer, G. *Sol-Gel Science: The Physics and Chemistry of Sol-Gel Processing*; Academic Press: San Diego, CA, USA, 1989.
20. Catauro, M.; Bollino, F.; Giovanardi, R.; Veronesi, P. Modification of Ti6Al4V implant surfaces by biocompatible TiO<sub>2</sub>/PCL hybrid layers prepared via sol-gel dip coating: Structural characterization, mechanical and corrosion behavior. *Mater. Sci. Eng. C* **2017**, *74*, 501–507. [[CrossRef](#)]
21. Catauro, M.; Bollino, F.; Papale, F.; Ferrara, C.; Mustarelli, P. Silica-polyethylene glycol hybrids synthesized by sol-gel: Biocompatibility improvement of titanium implants by coating. *Mater. Sci. Eng. C* **2015**, *55*, 118–125. [[CrossRef](#)] [[PubMed](#)]



22. Dehghanghadikolaei, A.; Ibrahim, H.; Amerinatanzi, A.; Hashemi, M.; Moghaddam, N.S.; Elahinia, M. Improving corrosion resistance of additively manufactured nickel–titanium biomedical devices by micro-arc oxidation process. *J. Mater. Sci.* **2019**, *54*, 7333–7355. [[CrossRef](#)]
23. Fahmi, A.; Abdullah, S.; Amin, F.; Ali, A. Precursor selection for sol–gel synthesis of titanium carbide nanopowders by a new cubic fuzzy multi-attribute group decision-making model. *J. Intell. Syst.* **2017**, *15*, 145–167. [[CrossRef](#)]
24. Roehling, S.; Gahlert, M.; Janner, S.; Meng, B.; Woelfler, H.; Cochran, D. Ligature-Induced Peri-implant Bone Loss Around Loaded Zirconia and Titanium implants. *Int. J. Oral Maxillofac. Implant* **2019**. [[CrossRef](#)]
25. Oliver, W.C.; Pharr, G.M. An improved technique for determining hardness and elastic modulus using load and displacement sensing indentation experiments. *J. Mater. Res.* **1992**, *7*, 1564–1583. [[CrossRef](#)]
26. Kokubo, T.; Takadama, H. How useful is SBF in predicting in vivo bone bioactivity? *Biomaterials* **2006**, *27*, 2907–2915. [[CrossRef](#)] [[PubMed](#)]
27. Catauro, M.; Barrino, F.; Poggetto, G.D.; Crescente, G.; Piccolella, S.; Pacifico, S. Chlorogenic acid entrapped in hybrid materials with high PEG content: A strategy to obtain antioxidant functionalized biomaterials? *Materials* **2019**, *12*. [[CrossRef](#)]
28. Catauro, M.; Tranquillo, E.; Risoluti, R.; Cipriotti, S.V. Sol-Gel synthesis, spectroscopic and thermal behavior study of SiO<sub>2</sub>/PEG composites containing different amount of chlorogenic acid. *Polymers* **2018**, *10*. [[CrossRef](#)]
29. Yoshino, H.; Kamiya, K.; Nasu, H. IR study on the structural evolution of sol-gel derived SiO<sub>2</sub> gels in the early stage of conversion to glasses. *J. Non-Cryst. Solids* **1990**, *126*, 68–78. [[CrossRef](#)]
30. Catauro, M.; Tranquillo, E.; Dell’Era, A.; Tuffi, R.; Vecchio Cipriotti, S. Thermal behavior and structural study of ZrO<sub>2</sub>/poly(ε-caprolactone) hybrids synthesized via sol-gel route. *Ceram. Int.* **2019**, *45*, 2771–2778. [[CrossRef](#)]
31. Ramesh, S.; Kim, H.S.; Lee, Y.-J.; Hong, G.-W.; Jung, D.; Kim, J.-H. Synthesis of cellulose-L-tyrosine-SiO<sub>2</sub>/ZrO<sub>2</sub> hybrid nanocomposites by sol-gel process and its potential. *Int. J. Precis. Eng. Manuf.* **2017**, *18*, 1297–1306. [[CrossRef](#)]
32. Miller, J.B.; Rankin, S.E.; Ko, E. Strategies in controlling the homogeneity of zirconia-silica aerogels: Effect of preparation on textural and catalytic properties. *J. Catal.* **1994**, *148*, 673–682. [[CrossRef](#)]
33. Wu, Z.-G.; Zhao, Y.-X.; Liu, D.-S. The synthesis and characterization of mesoporous silica–zirconia aerogels. *Microporous Mesoporous Mater.* **2004**, *68*, 127–132. [[CrossRef](#)]
34. Catauro, M.; Bollino, F.; Papale, F.; Giovanardi, R.; Veronesi, P. Corrosion behavior and mechanical properties of bioactive sol-gel coatings on titanium implants. *Mater. Sci. Eng. C* **2014**, *43*, 375–382. [[CrossRef](#)] [[PubMed](#)]
35. de Assis, S.L.; Wolyneć, S.; Costa, I. Corrosion characterization of titanium alloys by electrochemical techniques. *Electrochim. Acta* **2006**, *51*, 1815–1819. [[CrossRef](#)]
36. Cheng, X.; Roscoe, S.G. Corrosion behavior of titanium in the presence of calcium phosphate and serum proteins. *Biomaterials* **2005**, *26*, 7350–7356. [[CrossRef](#)] [[PubMed](#)]
37. Kokubo, T.; Ito, S.; Huang, Z.; Hayashi, T.; Sakka, S.; Kitsugi, T.; Yamamuro, T. Ca, P-rich layer formed on high-strength bioactive glass-ceramic A-W. *J. Biomed. Mater. Res.* **1990**, *24*, 331–343. [[CrossRef](#)] [[PubMed](#)]
38. Xu, J.; Wang, Y.; Huang, Y.; Cheng, H.; Seo, H.J. Surface reactivity and hydroxyapatite formation on Ca<sub>5</sub>MgSi<sub>3</sub>O<sub>12</sub> ceramics in simulated body fluid. *Appl. Surf. Sci.* **2017**, *423*, 900–908. [[CrossRef](#)]
39. Kokubo, T.; Kushitani, H.; Sakka, S.; Kitsugi, T.; Yamamuro, T. Solutions able to reproduce in vivo surface-structure changes in bioactive glass-ceramic A-W3. *J. Biomed. Mater. Res.* **1990**, *24*, 721–734. [[CrossRef](#)]

